ChemPubSoc Europe
DOI: 10.1002/cphc.201402750
CHEMPHYSCHEM
Articles

Special Issue

Difluorinated 6,13-Bis(triisopropylsilylethynyl)pentacene: Synthesis, Crystallinity, and Charge-Transport Properties

Chang-Hyun Kim,*[a, d] Htay Hlaing,[b] Marcia M. Payne,[c] Sean R. Parkin,[c] John E. Anthony,[c] and Ioannis Kymissis*[b]

Fluorination has been demonstrated to improve stability and processing in thiophene-containing small-molecule semiconductors. Here, the impact of partial fluorination on these parameters in a pentacene derivative is examined. Although the improvement in photostability is not as dramatic, there is a clear improvement in the stability of the chromophore upon fluorination. The improvement in processability is more dramatic; devices formed by spin-coating with the fluorinated derivative perform substantially better than those formed from the nonfluorinated compound.

1. Introduction

Organic semiconductors offer a fascinating platform for studying the impact of small changes in molecular functionalization on properties as diverse as crystallization rate, photo-stability, crystal packing, and charge-transport properties. In anthradithiophene-based chromophores, for example, it has been shown that the addition of just two fluorine substituents both dramatically enhanced the stability of the semiconductor[1] and enhanced crystallization rates to allow formation of crystalline films with good semiconductor performance using techniques such as spin-coating.[2] We were curious whether this partial-fluorination strategy provided a general benefit to other acene-like chromophores; enhancement of stability of anthradithiophenes by fluorination likely arises from chemical “blocking” of the most-reactive thiophene positions (Figure 1). In chromophores without terminal thiophene moieties, such blocking would not be operative. Furthermore, simple difluorination would likely yield a mixture of isomers, which might further complicate crystallization.

In this study, we report on the material and device properties of a difluorinated 6,13-bis(triisopropylsilylethynyl)pentacene (diF-TIPS-Pn; Figure 1). This new organic semiconductor has excellent solubility and crystallizes rapidly, enabling the spin-casting deposition of an active channel layer for organic field-effect transistors (OFETs). We investigated the characteristic crystal growth upon solvent drying by means of polarized optical microscopy, and the nanostructure of the semiconductor thin films were analyzed using grazing-incidence wide-angle X-ray scattering (GIWAXS) measurements. OFETs are used as a platform for understanding the electrical transport properties of the gate-controlled charge carriers in diF-TIPS-Pn. Upon presenting the data from a device based on this material, we address the limitation of the simplified parameter extraction model, and provide a comparison of several advanced approaches.

2. Results and Discussion

2.1. Synthesis and Material Characteristics

The difluorinated acene was easily synthesized using standard chemistry protocols. Starting from the commercially available 4-fluoro-*o*-xylene, bromination followed by Cava reaction yielded the intermediate pentacene quinone (Scheme 1). Ethynylation followed by deoxygenation provided diF-TIPS-Pn in good yield.

The photostability of the fluorinated pentacene was studied in 0.5 wt% solutions in toluene, and compared with similar solutions of the nonfluorinated TIPS-Pn. Absorption spectra of the solutions were measured every 2 h until the solution half-life could be obtained (Figure 2). For TIPS-Pn, a half-life of approximately 4 h was extracted from this study, whereas diF-TIPS-Pn exhibited a half-life of >6 h under identical conditions. Although the 50% improvement in half-life is not as dramatic as that seen for the corresponding anthradithiophenes, it demonstrates that partial fluorination does improve solution stability, likely by hindering oxidative decomposition pathways.

[a] Dr. C.-H. Kim
LPICM, Ecole Polytechnique, CNRS
91128 Palaiseau (France)
E-mail: chang-hyun.kim@polytechnique.edu

[b] Dr. H. Hlaing, Prof. I. Kymissis
Department of Electrical Engineering
Columbia University
New York, NY 10027 (USA)
E-mail: johnkym@ee.columbia.edu

[c] Dr. M. M. Payne, Dr. S. R. Parkin, Prof. J. E. Anthony
Department of Chemistry
University of Kentucky
Lexington, KY 40506 (USA)

[d] Dr. C.-H. Kim
Current address:
School of Materials Science and Engineering
Gwangju Institute of Science and Technology
Gwangju 500-712 (Republic of Korea)

An invited contribution to a Special Issue on Organic Electronics

© 2015 Wiley-VCH Verlag GmbH & Co. KGaA, Weinheim

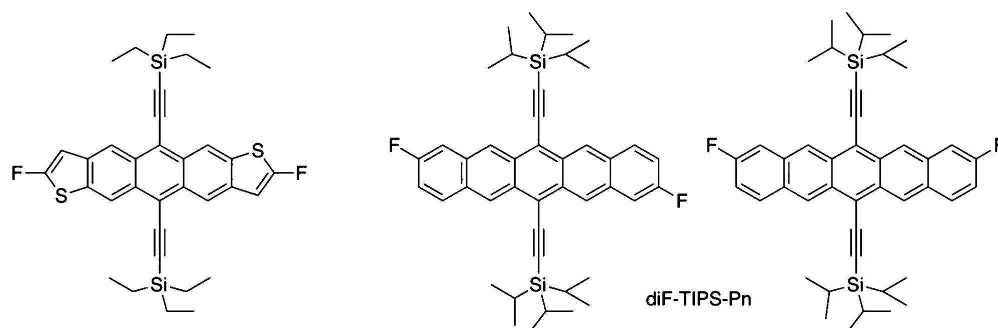

Figure 1. Fluorinated anthradithiophene (left), and the mixture of diF-TIPS-Pn isomers.

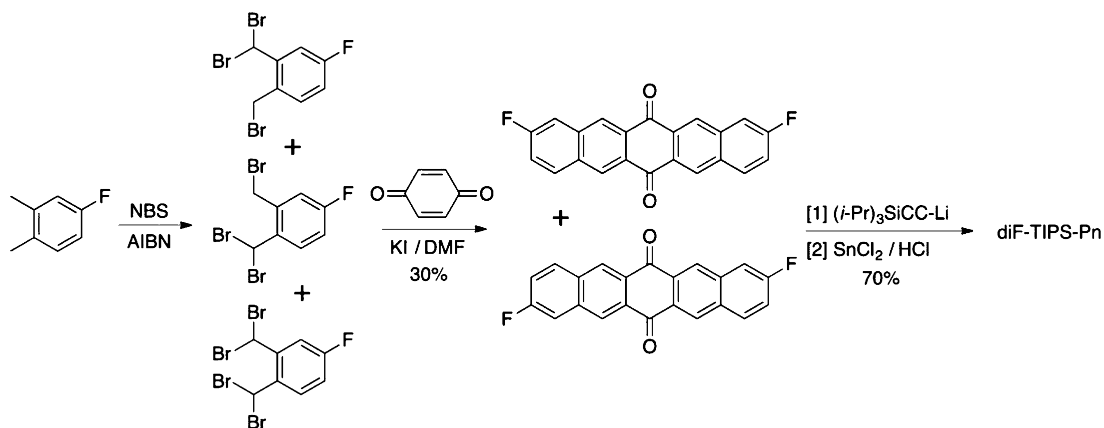

Scheme 1. Synthesis of diF-TIPS-Pn.

X-ray crystallographic analysis of diF-TIPS-Pn was performed, demonstrating that the material adopts a 2D "brickwork" crystal packing nearly identical to that determined for TIPS Pn,[3] as shown in Figure 3. It is obvious that the fluorine atoms are scrambled over all possible positions in the solid state—a function of the fact that a fluorine substituent is similar in size to a hydrogen atom. More importantly, it is clear that fluorination had no impact on the crystal packing—the overall arrangements for TIPS-Pn and diF-TIPS-Pn are essentially identical, with no changes in molecular orientation or carbon–carbon contacts; even the disorder of the single isopropyl group on each silane is nearly identical for the two compounds.

2.2. Contact-Induced Crystal Growth

Organic crystals are formed by weak van der Waals forces. This underlines the significant impact the substrate chemistry has on the arrangement of deposited molecules, because substantial substrate–molecule interactions can be comparable to, or even dominant over, intermolecular forces.[4,5] As efficient charge transport necessitates a high degree of solid-state order and ideal orientation of the crystallites,[6,7] understanding and exploiting the surface properties for obtaining a desired film structure is of great importance.

In complete OFET devices, a semiconductor layer sits on the SiO_2 channel region and on the chemically functionalized Au source/drain electrodes as illustrated in Figure 4a. Figure 4b shows that the morphology is significantly different on these two characteristic surfaces. Pentafluorobenzenethiol (PFBT) is a widely used self-assembled monolayer (SAM) material for charge-injection contacts.[8–11] Previously, extensive studies were conducted on difluorinated 5,11-bis(triethylsilylethynyl)-anthradithiophene films grown on PFBT-treated Au. They suggested that fluorine–fluorine and sulfur–fluorine interactions between the semiconductor and the electrode promote molecular packing, as evidenced by the alignment of crystalline domains along the electrode edges.[8,12–14] In our diF-TIPS-Pn devices, similar phenomena were observed (Figure 4b), by which nucleation is predominantly initiated on the electrode regions with the growth extending laterally to fill the channel. A noticeable optical contrast inversion upon rotation of the sample (Figure 4c) characterized the highly ordered crystalline domains.[15,16]

From the images in Figure 4b,c, it can be inferred that the width and length of the grains in the channel are restricted by the nucleation density on the electrodes and the channel length (*L*), respectively. Moving farther away from an electrode, more spatially distributed nucleation on SiO_2 were observed, which eventually creates zones with large spherulitic domains (Figure 4d).[17] This image reveals the exceptional ability of diF-TIPS-Pn to strongly correlate and form crystalline domains under solution casting. However, we cannot simply expect that

© 2015 Wiley-VCH Verlag GmbH & Co. KGaA, Weinheim

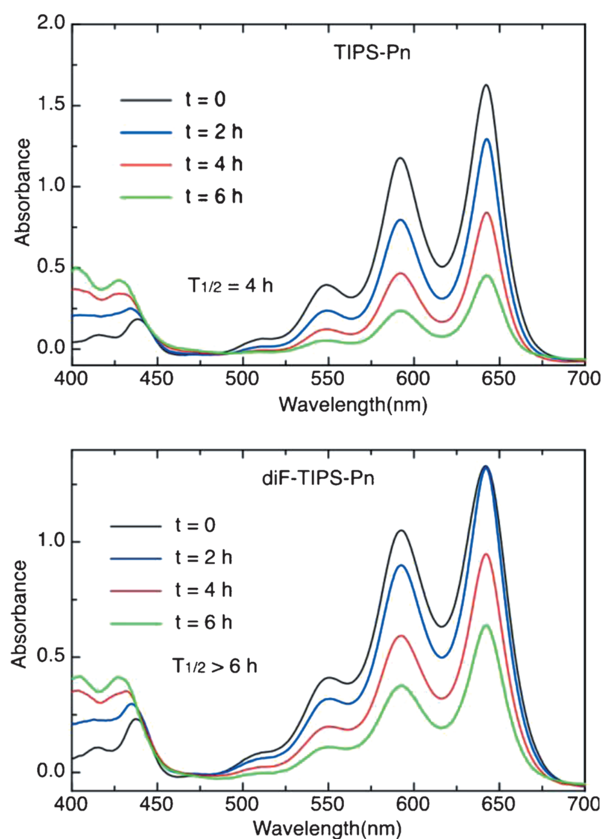

Figure 2. Decomposition of TIPS-Pn (top) and diF-TIPS-Pn (bottom) in solution, monitored by absorption spectroscopy.

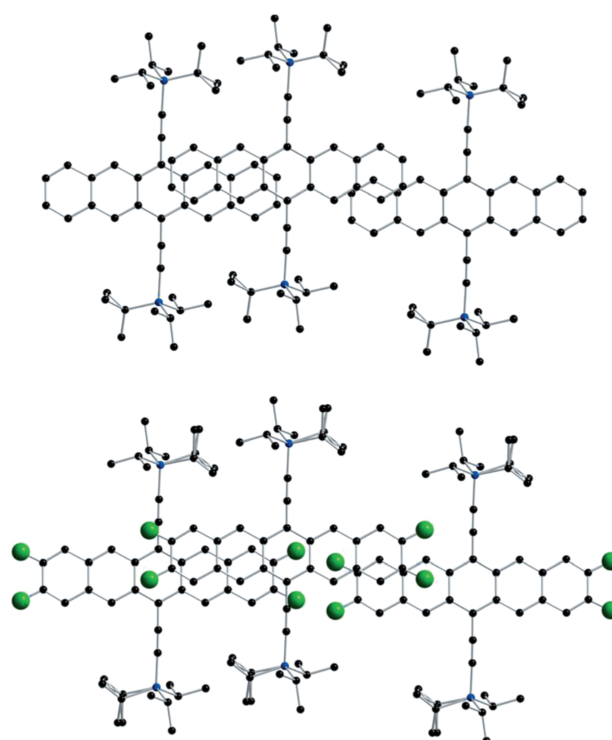

Figure 3. A comparison of the crystal packing of TIPS-Pn (top) and diF-TIPS-Pn (bottom).

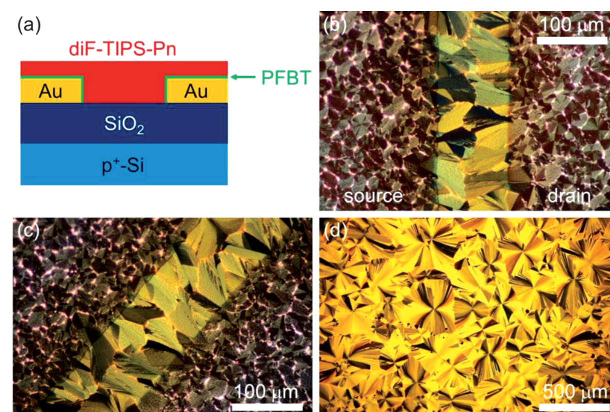

Figure 4. a) OFET device architecture and materials. b) Optical image under crossed polarizers showing the morphology of a spin-cast diF-TIPS-Pn film. c) Image of the same region as (b) with the sample rotated with respect to the fixed polarizing angles. d) Polarized optical image at lower magnification on a far-electrode SiO_2 region.

long-range (channel-scale) charge transport would be superior within this region; the arbitrary orientation of domains results in a number of high-angle grain boundaries that render intergrain current flow inefficient.[18] Although smaller, the contact-grown grains in Figure 4b,c are "in-plane" directional. In practice, charge carriers encounter only one "mid-channel" boundary, and even this boundary is low-angled and thus easy to pass through.[18]

2.3. GIWAXS

2D GIWAXS is a powerful method to quantitatively determine the nanoscale crystalline structures and substrate-relative domain orientations, and its application to organic electronic materials has recently received growing attention.[19–24]

In order to investigate the crystallinity of the diF-TIPS-Pn films on morphologically distinguishable PFBT–Au and SiO_2 regions, GIWAXS measurements were separately conducted on these two locations. The 2D scattering patterns (Figure 5a,b) feature strikingly well-defined peaks including many high-order peaks, characteristic of a well-defined molecular crystal structure. A spin-cast organic film tends to poorly crystallize due to fast drying of the solvent.[25] Therefore, we estimate that diF-TIPS-Pn molecules have an outstanding ability to crystallize, and the fluorinated arenethiol layer coating the Au surface plays an additional role in generating a highly crystalline semiconducting thin film.

The scattering peaks do not show substantial angular spreading, indicating that there is a well-defined preferential orientation of the crystallites with respect to the substrate. The position of the peaks corresponds to the so-called "edge-on" motif, as evidenced by the pronounced (00 *l*) peaks along the q_z axis.[26] It is important to note that efficient lateral conduction for OFETs is achieved with these edge-on crystals due to

© 2015 Wiley-VCH Verlag GmbH & Co. KGaA, Weinheim

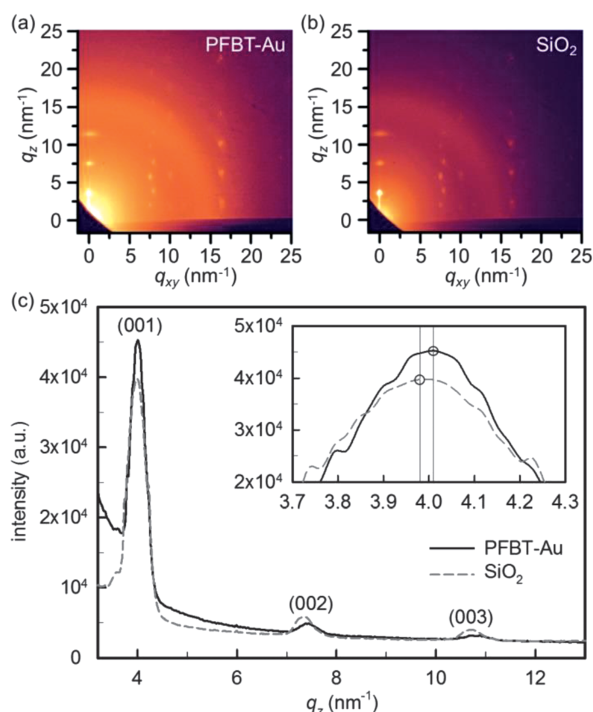

Figure 5. 2D GIWAXS images of the spin-cast diF-TIPS-Pn film on a) PFBT–Au and b) SiO_2. c) The out-of-plane profiles at $q_{xy}=0$; inset: magnification of the (001) peaks; the maximum data points of the two profiles are marked by circles.

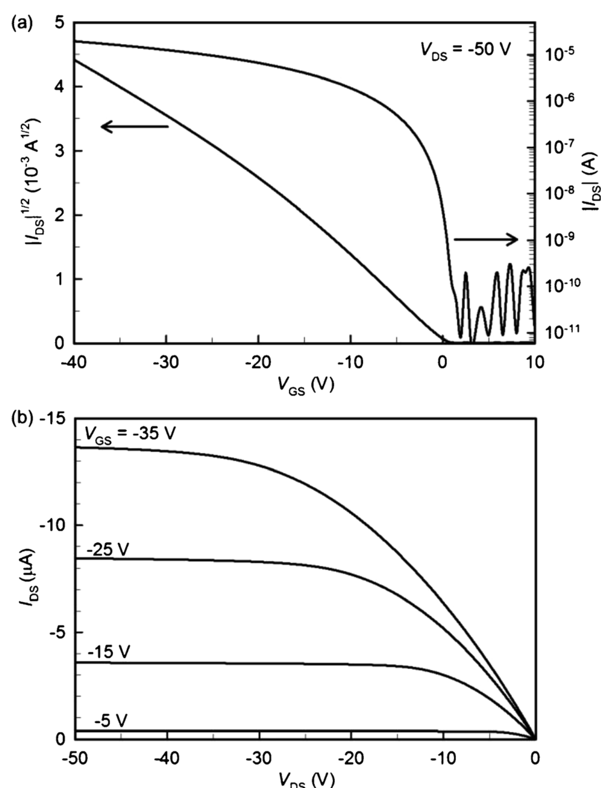

Figure 6. a) Saturation-regime transfer characteristic of a diF-TIPS-Pn transistor on a semi-log scale and the square root of the same data on a linear scale. b) Output characteristics of the same device. This OFET has $W=3000$ μm and $L=100$ μm.

the significant π–π overlap aligned in the transport direction. Figure 5c shows a comparison of the extraction of the out-of-plane scattering profile of the two substrates. Although the peak distribution looks overall similar on PFBT–Au and SiO_2, the exact q_z values resulting in the series of (001) peaks were slightly smaller for SiO_2. The extracted q_{001} value is 4.01 nm^{-1} for the crystals on PFBT–Au and 3.98 nm^{-1} for those on SiO_2 (Figure 5c). The corresponding interlayer spacing $d_{001}=2\pi/q_{001}$ is 1.56 nm for PFBT–Au and 1.57 nm for SiO_2. Although not significant, this difference can arise from the stronger attraction of the PFBT–Au surface for the diF-TIPS-Pn molecules upon crystallization, eventually creating more condensed regions.

2.4. OFET Analysis

The charge-transport properties of diF-TIPS-Pn were studied by measuring current–voltage (*I*–*V*) characteristics of the spin-cast OFETs. As the on-state current flow is attributed to the controllable (i.e. quantifiable) gate-induced charge carriers, OFETs provide practical access to the charge-carrier mobility (μ) from *I*–*V* characteristics.[27] The *I*–*V* data from a representative diF-TIPS-Pn transistor are shown in Figure 6. The channel width (*W*) and *L* of this transistor are 3000 and 100 μm, respectively. The transfer characteristic (Figure 6a) shows a large modulation of drain current (I_{DS}) by the gate voltage (V_{GS}) by a factor of the order of 10^6, a property necessary for low-leakage switching applications. The on state observed at negative V_{GS} values indicates the *p*-type field-effect behavior achieved by holes injected from the Au electrodes. The output curves [I_{DS} vs. drain voltage (V_{DS}); Figure 6b] feature an almost ideal linear-to-saturation transition, suitable for applications such as organic light-emitting diode (OLED) driving circuits.[28]

Related to the virtually unlimited range of semiconductor materials and device structures, there is still no universal description for the device operation of OFETs. Likely due to its simplicity in implementation, the major choice of the research community has been to adopt the quadratic MOSFET *I*–*V* model based on the gradual channel approximation.[27,29,30] However, it is worth questioning the wide applicability of this model to OFETs for the following reasons. Structural and energetic disorder is characteristic of organic semiconductors, which dictates a strong dependence of μ on the applied V_{GS}.[31–33] Also, the ideal MOSFET model does not include contact resistance (R_c), which generally exists due to a substantial charge-injection barrier at direct metal–semiconductor junctions in OFETs.[34–36] From a behavioral point of view, both aspects (V_{GS}-dependent μ and the R_c effect) manifest themselves by a deviation of a measured saturation-regime $|I_{DS}|^{1/2}$ versus V_{GS} curve from a perfectly straight line.[37–40] Our OFET also exhibits such a trend (Figure 6a), and therefore estimating a unique slope for the single μ value is not possible. Hereinafter, we suggest alternative ways to extract μ values that allow the utilization of the entire range of transfer curves with a more physically based description. We will summarize the as-

© 2015 Wiley-VCH Verlag GmbH & Co. KGaA, Weinheim

sumptions behind each model, and explain their implementation and relative advantages and drawbacks.

The first method is based on the second derivative of the transfer curves. Essentially, the same form of the saturation-regime MOSFET equation is used with an additional freedom in the variation of μ with V_{GS}. We define μ_{SD} as the mobility extracted by the second derivative and write Equation (1) for the *p*-type operation:

$$I_{DS} = -\frac{W}{2L}\mu_{SD}C_i(V_{GS} - V_T)^2 \quad (1)$$

where C_i is the gate insulator capacitance per unit area and V_T is the threshold voltage. Although not often explicitly mentioned,[10,41] the derivations lead to a simple equation only by assuming a weak V_{GS}-dependence, which ignores the $d\mu_{SD}/dV_{GS}$ and $d^2\mu_{SD}/dV_{GS}{}^2$ terms. Therefore, Equation (2) should be considered as an approximation:

$$\frac{d^2I_{DS}}{dV_{GS}^2} \approx -\frac{W}{L}\mu_{SD}C_i \quad (2)$$

rearrangement of which for μ_{SD} gives Equation (3):

$$\mu_{SD} \approx \frac{d^2I_{DS}}{dV_{GS}^2} \times -\frac{L}{W} \times \frac{1}{C_i} \quad (3)$$

A major advantage of this method is to estimate the V_{GS} dependence of μ without simultaneous estimation of V_T. Similarly to μ, the V_T can be extracted by various methods that produce potentially different values.[42,43] Therefore, the elimination of V_T by two derivations from Equation (1) allows one to be freed from the additional complications of the choice of method and voltage range for V_T extraction. However, the method tends to amplify the measurement noise because mathematical derivations are involved (Figure 7a). As superposed here, a data-smoothing algorithm can be applied when, for instance, the functional form of μ versus V_{GS} is to be precisely modeled.

The second method relies upon a predetermined V_T value, so we term μ_{TH} (TH = threshold) as the mobility extracted this way. We replace μ_{SD} by μ_{TH} in Equation (1). The difference consists in the direct arrangement for μ_{TH}, leading to Equation (4):

$$\mu_{TH} = I_{DS} \times -\frac{2L}{W} \times \frac{1}{C_i} \times \frac{1}{(V_{GS} - V_T)^2} \quad (4)$$

Equation (4) clearly shows that the value of V_T should be first determined to calculate the value of μ_{TH} at each V_{GS} from a measured saturation-regime transfer curve. As shown in Figure 7b, noise-free estimation of the V_{GS}-dependent mobility is possible. Furthermore, additional physical correlation can be introduced because the accumulated channel charge density is proportional to the gate overdrive voltage $V_{GS}-V_T$ [Eq. (5)]:

$$Q_{ch} = -C_i(V_{GS} - V_T) \quad (5)$$

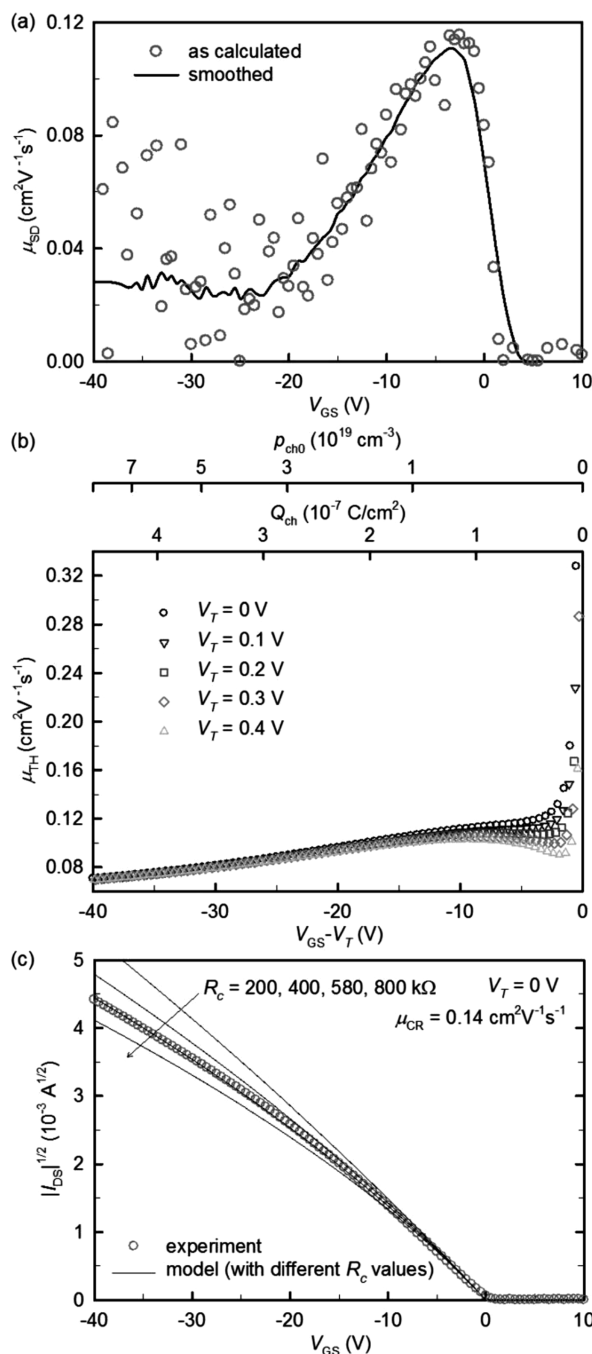

Figure 7. Calculation and visualization for the different parameter extraction schemes applied to the transfer curve shown in Figure 6a. a) Second-derivative method, b) threshold-voltage method, and c) contact-resistance method.

where Q_{ch} is the capacitively induced hole charge density per unit area in the organic channel. By assuming a Mott–Gurney-type charge distribution (for a semi-infinite metal–insulator junction), the interfacial channel hole density per volume p_{ch0} can be calculated [Eq. (6)]:[36]

$$p_{ch0} = \frac{Q_{ch}^2}{2\varepsilon_S kT} = \frac{C_i^2(V_{GS} - V_T)^2}{2\varepsilon_S kT} \quad (6)$$

© 2015 Wiley-VCH Verlag GmbH & Co. KGaA, Weinheim

where ε_s is the semiconductor permittivity, k is the Boltzmann constant, and T is the absolute temperature. The calculated μ_{TH} of our diF-TIPS-Pn transistor as a function of $V_{GS}-V_T$, Q_{ch}, and p_{ch0} is shown in Figure 7b. We used $\varepsilon_s=3.5\times\varepsilon_0$[44] and $T=$ 300 K (ε_0 is the vacuum permittivity). As the last term in Equation (4) goes to infinity as $V_{GS}\rightarrow V_T$, the result is highly sensitive to the value of V_T especially near $V_{GS}-V_T=0$ V. We also note that the locally high values at the first one or two data points nearest to $V_{GS}-V_T=0$ V are due to the same specificity of the calculation.

The third method includes R_c in the I–V model, and the corresponding mobility is termed μ_{CR} (CR = contact resistance). As proposed by Natali and co-workers,[45] a contact voltage drop at the source electrode accounts for the reduction in current, and the self-consistent saturation-regime drain current I_{CR} can be written as Equation (7):

$$I_{CR}=\frac{V_{GS}-V_T}{R_c}+\frac{L}{W\mu_{CR}C_iR_c^2}\left[-1+\sqrt{1-\frac{2W}{L}\mu_{CR}C_iR_c(V_{GS}-V_T)}\right] \quad (7)$$

Due to the interdependency between μ_{CR} and R_c, the extraction of separate parameters at each V_{GS} cannot be achieved with a single device. In other words, either μ_{CR} or R_c should have a known functional V_{GS} dependence to assign a functional freedom to the other and extract its unknown V_{GS} dependence. Nonetheless, a broad range within the transfer curve of our OFET can be sufficiently well fitted by using constant μ_{CR} and R_c values ($R_c=580$ kΩ curve in Figure 7c), which might serve as an approximation to their relatively weak V_{GS} dependence. The extracted μ_{CR} value of 0.14 $cm^2V^{-1}s^{-1}$ averages the charge-transport property of the diF-TIPS-Pn channel unaffected by the contact-related current reduction, and this value is close to the μ_{SD} or μ_{TH} under low $|V_{GS}|$. Therefore, we observe an enhancement in OFET performance as compared to the reported μ value of spin-cast TIPS-Pn transistors of <0.04 $cm^2V^{-1}s^{-1}$.[46] Considering negligible contribution of the fluorine atoms to the packing structure (Figure 3), the contact-induced self-assembly-promoting in-plane ordering of crystallites is expected to be the major factor in the improvement. Figure 7c also contains the calculated transfer curves according to Equation (7), with adjacent R_c values to visualize the pronounced bending with increasing R_c. Note that recent reports on high-mobility materials often showed a similar deviation, highlighting the inability of the injection contacts to provide sufficient charge carriers that can fully utilize the highly conductive channel.[38–40,47]

3. Conclusions

We have investigated a novel semiconductor, diF-TIPS-Pn, with a particular focus on its application to OFETs. The chemical tuning of the widely studied TIPS-Pn was inspired by the benchmark already set with anthradithiophene derivatives; we observed a generalized enhancement of the stability of the material by fluorination, even in the absence of thiophene moieties in the core structure. The excellent solubility of diF-TIPS-Pn enabled impressive processability for device manufacturing, and OFETs fabricated using spin-casting provided a platform for monitoring the thin-film microstructure and the charge-transport properties. The polarized optical microscopy and X-ray-based structural analysis showed that fluorination on the semiconductor activates contact-induced crystal growth along SAM-functionalized Au surfaces, generating well-aligned crystallites optimized for in-plane electrical conduction. A rigorous analysis of the mobility extraction methods was provided, for highlighting the necessity of careful inspection of measured transfer curves that exhibit substantial nonideality. In the framework of charge-transport physics within a uniform medium, μ_{SD}- or μ_{TH}-based methods can be more reliable if upward bending (of a $|I_{DS}|^{1/2}$ vs. V_{GS} curve) is pronounced, because of the compatibility with the hopping or trap-dominated transport models. Downward bending is generally observed for high-performance semiconductors, and this was also the case for our diF-TIPS-Pn transistor. R_c is regarded as the major reason for this deviation, and we showed that an assumption of constant R_c and μ_{CR} can sufficiently well describe the overall transfer characteristic. Our results deliver a comprehensive understanding of a newly proposed organic semiconductor, from chemical synthesis to device analysis, and they make a strong case for a rational molecular design strategy.

Experimental Section

Device Fabrication

OFETs were fabricated according to the structure in Figure 4a. A heavily doped p-type Si wafer covered with 300 nm SiO_2 was used as a substrate and a common gate-electrode/insulator platform. The substrate was subsequently cleaned with acetone, isopropanol, and distilled water. A Cr adhesion layer (5 nm) and Au source/drain electrodes (35 nm) were deposited by vacuum evaporation through a shadow mask. The sample was then immersed into a PFBT solution (10 mM in isopropanol) for 1 h, followed by rinsing with pure isopropanol and blow-drying with nitrogen. diF-TIPS-Pn powder was dissolved in 1,2,3,4-tetrahydronaphthalene (17 $mg\,mL^{-1}$). The semiconductor solution was spin-cast at 1000 rpm for 30 s, and the fabrication was completed with an immediate annealing of the samples on a hot plate at 100 °C for 30 min.

Electrical Characterization

Current–voltage characteristics of the OFETs were recorded using a semiconductor characterization system (Keithley 4200) in the dark at room temperature.

Optical Characterization

Optical microscopy images were acquired with a Nikon Eclipse E600FN system under crossed polarizers. A Canon Rebel T3i EOS 600D digital single-lens reflex camera was mounted onto the microscope and computer-controlled for high-quality imaging.

© 2015 Wiley-VCH Verlag GmbH & Co. KGaA, Weinheim

GIWAXS Measurements

GIWAXS measurements were performed at the undulator-based X9 beam line at the National Synchrotron Light Source (NSLS), Brookhaven National Laboratory. The incident X-ray beam with photon energy of 14.0 keV (wavelength 0.08856 nm) was collimated using slits and focused onto the sample position using Kirkpatrick–Biaz mirrors, providing a beam size of 100 μm horizontal width and 50 μm vertical width. The samples were fixed to the sample stage located inside the vacuum chamber (pressure ≈40 Pa) and grazing incidence with respect to the incident X-ray was obtained by titling the stage. 2D scattering images were collected using a fiber-coupled CCD area detector (Photonic Science, Mountfield, UK, pixel size 0.102 mm), positioned 217 mm from the center of the sample stage. Measurements were performed at a variety of incident angles; the results presented in the manuscript were taken at the incident angle of 0.12°. Data conversion to q-space was accomplished by calibration using silver behenate powder.

Acknowledgements

C.-H.K. acknowledges financial support from the Ecole Polytechnique Postdoctoral Research Grant and administrative support from the Alliance Program. I.K., H.H., and overall project coordination, as well as sample growth and characterization were supported as part of the Center for Re-Defining Photovoltaic Efficiency Through Molecular-Scale Control, an Energy Frontier Research Center funded by the U.S. Department of Energy (DOE), Office of Science, Office of Basic Energy Sciences under Award DE-SC0001085. J.E.A. and M.M.P. thank the National Science Foundation (CMMI-1255494) for support of crystalline organic semiconductor development.

Keywords: charge transport · crystal structure · organic field-effect transistors · pentacenes · semiconductors

[1] S. Subramanian, S. K. Park, S. R. Parkin, V. Podzorov, T. N. Jackson, J. E. Anthony, *J. Am. Chem. Soc.* **2008**, *130*, 2706 – 2707.
[2] S. K. Park, D. A. Mourey, S. Subramanian, J. E. Anthony, T. N. Jackson, *Appl. Phys. Lett.* **2008**, *93*, 043301 – 043303.
[3] J. E. Anthony, J. S. Brooks, D. L. Eaton, S. R. Parkin, *J. Am. Chem. Soc.* **2001**, *123*, 9482 – 9483.
[4] R. Ruiz, D. Choudhary, B. Nickel, T. Toccoli, K.-C. Chang, A. C. Mayer, P. Clancy, J. M. Blakely, R. L. Headrick, S. Iannotta, G. G. Malliaras, *Chem. Mater.* **2004**, *16*, 4497 – 4508.
[5] S. Y. Yang, K. Shin, C. E. Park, *Adv. Funct. Mater.* **2005**, *15*, 1806 – 1814.
[6] A. A. Virkar, S. Mannsfeld, Z. Bao, N. Stingelin, *Adv. Mater.* **2010**, *22*, 3857 – 3875.
[7] H. N. Tsao, K. Mullen, *Chem. Soc. Rev.* **2010**, *39*, 2372 – 2386.
[8] D. J. Gundlach, J. E. Royer, S. K. Park, S. Subramanian, O. D. Jurchescu, B. H. Hamadani, A. J. Moad, R. J. Kline, L. C. Teague, O. Kirillov, C. A. Richter, J. G. Kushmerick, L. J. Richter, S. R. Parkin, T. N. Jackson, J. E. Anthony, *Nat. Mater.* **2008**, *7*, 216 – 221.
[9] C. H. Kim, H. Hlaing, F. Carta, Y. Bonnassieux, G. Horowitz, I. Kymissis, *ACS Appl. Mater. Interfaces* **2013**, *5*, 3716 – 3721.
[10] X. Zhang, H. Bronstein, A. J. Kronemeijer, J. Smith, Y. Kim, R. J. Kline, L. J. Richter, T. D. Anthopoulos, H. Sirringhaus, K. Song, M. Heeney, W. Zhang, I. McCulloch, D. M. DeLongchamp, *Nat. Commun.* **2013**, *4*, 2238.
[11] H. Lee, Y. Zhang, L. Zhang, T. Mirabito, E. K. Burnett, S. Trahan, A. R. Mohebbi, S. C. B. Mannsfeld, F. Wudl, A. L. Briseno, *J. Mater. Chem. C* **2014**, *2*, 3361 – 3366.
[12] R. J. Kline, S. D. Hudson, X. Zhang, D. J. Gundlach, A. J. Moad, O. D. Jurchescu, T. N. Jackson, S. Subramanian, J. E. Anthony, M. F. Toney, L. J. Richter, *Chem. Mater.* **2011**, *23*, 1194 – 1203.
[13] R. Li, J. W. Ward, D.-M. Smilgies, M. M. Payne, J. E. Anthony, O. D. Jurchescu, A. Amassian, *Adv. Mater.* **2012**, *24*, 5553 – 5558.
[14] J. W. Ward, M. A. Loth, R. J. Kline, M. Coll, C. Ocal, J. E. Anthony, O. D. Jurchescu, *J. Mater. Chem.* **2012**, *22*, 19047 – 19053.
[15] J. Rivnay, L. H. Jimison, J. E. Northrup, M. F. Toney, R. Noriega, S. Lu, T. J. Marks, A. Facchetti, A. Salleo, *Nat. Mater.* **2009**, *8*, 952 – 958.
[16] H. T. Yi, M. M. Payne, J. E. Anthony, V. Podzorov, *Nat. Commun.* **2012**, *3*, 1259.
[17] S. S. Lee, M. A. Loth, J. E. Anthony, Y.-L. Loo, *J. Am. Chem. Soc.* **2012**, *134*, 5436 – 5439.
[18] S. S. Lee, J. M. Mativetsky, M. A. Loth, J. E. Anthony, Y.-L. Loo, *ACS Nano* **2012**, *6*, 9879 – 9886.
[19] H. Hlaing, X. Lu, T. Hofmann, K. G. Yager, C. T. Black, B. M. Ocko, *ACS Nano* **2011**, *5*, 7532 – 7538.
[20] X. Lu, H. Hlaing, D. S. Germack, J. Peet, W. H. Jo, D. Andrienko, K. Kremer, B. M. Ocko, *Nat. Commun.* **2012**, *3*, 795.
[21] C.-H. Kim, H. Hlaing, S. Yang, Y. Bonnassieux, G. Horowitz, I. Kymissis, *Org. Electron.* **2014**, *15*, 1724 – 1730.
[22] S. C. B. Mannsfeld, M. L. Tang, Z. Bao, *Adv. Mater.* **2011**, *23*, 127 – 131.
[23] A. Salleo, R. J. Kline, D. M. DeLongchamp, M. L. Chabinyc, *Adv. Mater.* **2010**, *22*, 3812 – 3838.
[24] J. B. Kim, Z.-L. Guan, S. Lee, E. Pavlopoulou, M. F. Toney, A. Kahn, Y.-L. Loo, *Org. Electron.* **2011**, *12*, 1963 – 1972.
[25] K. C. Dickey, J. E. Anthony, Y. L. Loo, *Adv. Mater.* **2006**, *18*, 1721 – 1726.
[26] C.-H. Kim, H. Hlaing, M. M. Payne, K. G. Yager, Y. Bonnassieux, G. Horowitz, J. E. Anthony, I. Kymissis, *ChemPhysChem* **2014**, *15*, 2913 – 2916.
[27] C. H. Kim, Y. Bonnassieux, G. Horowitz, *IEEE Trans. Electron Devices* **2013**, *61*, 278 – 287.
[28] S. Kim, A. Konar, W.-S. Hwang, J. H. Lee, J. Lee, J. Yang, C. Jung, H. Kim, J.-B. Yoo, J.-Y. Choi, Y. W. Jin, S. Y. Lee, D. Jena, W. Choi, K. Kim, *Nat. Commun.* **2012**, *3*, 1011.
[29] W. Shockley, *Proc. IRE* **1952**, *40*, 1365 – 1376.
[30] G. Horowitz, *Adv. Mater.* **1998**, *10*, 365 – 377.
[31] G. Horowitz, *J. Appl. Phys.* **1999**, *85*, 3202.
[32] G. Horowitz, M. E. Hajlaoui, R. Hajlaoui, *J. Appl. Phys.* **2000**, *87*, 4456 – 4463.
[33] M. C. J. M. Vissenberg, M. Matters, *Phys. Rev. B* **1998**, *57*, 12964 – 12967.
[34] A. Kahn, N. Koch, W. Gao, *J. Polym. Sci. Part B* **2003**, *41*, 2529 – 2548.
[35] S. Braun, W. R. Salaneck, M. Fahlman, *Adv. Mater.* **2009**, *21*, 1450 – 1472.
[36] C. H. Kim, Y. Bonnassieux, G. Horowitz, *IEEE Trans. Electron Devices* **2012**, *60*, 280 – 287.
[37] D. Lehnherr, A. R. Waterloo, K. P. Goetz, M. M. Payne, F. Hampel, J. E. Anthony, O. D. Jurchescu, R. R. Tykwinski, *Org. Lett.* **2012**, *14*, 3660 – 3663.
[38] Y. Mei, M. A. Loth, M. Payne, W. Zhang, J. Smith, C. S. Day, S. R. Parkin, M. Heeney, I. McCulloch, T. D. Anthopoulos, J. E. Anthony, O. D. Jurchescu, *Adv. Mater.* **2013**, *25*, 4352 – 4357.
[39] Y. Diao, B. C. K. Tee, G. Giri, J. Xu, D. H. Kim, H. A. Becerril, R. M. Stoltenberg, T. H. Lee, G. Xue, S. C. B. Mannsfeld, Z. Bao, *Nat. Mater.* **2013**, *12*, 665 – 671.
[40] H. Chen, Y. Guo, G. Yu, Y. Zhao, J. Zhang, D. Gao, H. Liu, Y. Liu, *Adv. Mater.* **2012**, *24*, 4618 – 4622.
[41] A. L. Briseno, R. J. Tseng, M. M. Ling, E. H. L. Falcao, Y. Yang, F. Wudl, Z. Bao, *Adv. Mater.* **2006**, *18*, 2320 – 2324.
[42] A. Ortiz-Conde, F. J. García-Sánchez, J. Muci, A. Terán Barrios, J. J. Liou, C.-S. Ho, *Microelectron. Reliab.* **2013**, *53*, 90 – 104.
[43] D. Boudinet, G. Le Blevennec, C. Serbutoviez, J.-M. Verilhac, H. Yan, G. Horowitz, *J. Appl. Phys.* **2009**, *105*, 084510.
[44] C. H. Kim, O. Yaghmazadeh, D. Tondelier, Y. B. Jeong, Y. Bonnassieux, G. Horowitz, *J. Appl. Phys.* **2011**, *109*, 083710.
[45] D. Natali, L. Fumagalli, M. Sampietro, *J. Appl. Phys.* **2007**, *101*, 014501.
[46] Y.-H. Kim, Y. U. Lee, J.-I. Han, S.-M. Han, M.-K. Han, *J. Electrochem. Soc.* **2007**, *154*, H995 – H998.
[47] Y. Yuan, G. Giri, A. L. Ayzner, A. P. Zoombelt, S. C. B. Mannsfeld, J. Chen, D. Nordlund, M. F. Toney, J. Huang, Z. Bao, *Nat. Commun.* **2014**, *5*, 3005.

Received: October 24, 2014
Published online on January 15, 2015

© 2015 Wiley-VCH Verlag GmbH & Co. KGaA, Weinheim